

A dated volcano-tectonic deformation event in Jan Mayen causing landlocking of Arctic charr

EILIV LARSEN,^{1*} ASTRID LYSÅ,¹ ÁRMANN HÖSKULDSSON,² JAN G. DAVIDSEN,³ MARIE J. NADEAU,⁴ MICHAEL POWER,⁵ GEORGIOS TASSIS¹ and STEFAN WASTEGÅRD⁶

¹Geological Survey of Norway, Trondheim, Norway

²Nordic Volcanological Center, Institute of Earth Sciences, University of Iceland, Reykjavik Iceland

³NTNU University Museum, Norwegian University of Science and Technology, Trondheim, Norway

⁴The National Laboratory for Age Determination, Norwegian University of Science and Technology, Trondheim, Norway

⁵Department of Biology, University of Waterloo, Waterloo, ON, Canada

⁶Stockholm University, Department of Physical Geography, Stockholm, Sweden

Received 9 November 2020; Revised 22 January 2021; Accepted 24 January 2021

ABSTRACT: We provide the first documentation of tectonic deformation resulting from a volcanic eruption on the island of Jan Mayen. Vertical displacement of about 14 m southwest of the stratovolcano Beerenberg is associated with an eruption in AD 1732 on its southeastern flank. The age of the uplift event is bracketed by radiocarbon-dated driftwood buried by material deposited due to uplift, and by tephra from this eruption. Constraints, inferred from radiocarbon ages alone, allow for the possibility that uplift was completed prior to the AD 1732 eruption. However, the occurrence of tephra in the sediment column indicates that some displacement was ongoing during the eruption but ceased before the eruption terminated. We attribute the tectonic deformation to intrusion of shallow magma associated with the volcanic eruption. Our results complement previous studies of volcanic activity on Jan Mayen by providing precise age constraints for past volcanic activity. Also, it raises new hypotheses regarding the nature, timing and prevalence of precursor tectonic events to Jan Mayen eruptions. The uplift caused the complete isolation of a coastal lake by closing its outlet to the sea, thus landlocking the facultative migratory fish species Arctic charr (*Salvelinus alpinus*).

© 2021 The Authors. Journal of Quaternary Science Published by John Wiley & Sons Ltd.

KEYWORDS: AD 1732 volcanism; Jan Mayen; landlocked charr; stratigraphy; volcano-tectonic uplift

Introduction

Land surface processes interact with volcanic activity in a wide variety of environmental settings (Gudmundsson *et al.*, 2002; D'Argenio *et al.*, 2004; Smellie *et al.*, 2018; Pistolesi *et al.*, 2020). Such interactions are important to understand in volcanic terrains to elucidate their geological evolution (Manville *et al.*, 2009; Zernack *et al.*, 2011; Martí *et al.*, 2018; Nemeth and Palmer, 2019). Here we describe such processes on the volcanic island of Jan Mayen located at 71°N, 8°30'W in the Norwegian–Greenland Sea (Fig. 1A). All historical eruptions occurred along the flanks of the ice-covered stratovolcano Beerenberg (Fig. 1B), and some were close to Little Ice Age moraines. Gjerløw *et al.* (2015) documented the geographic distribution of a tephra from the AD 1732 hydromagmatic eruption, which formed the tuff cone Eggøya on the east coast of Jan Mayen (Fig. 1B). Three more eruptions (AD 1818, 1970 and 1985) are known (Scoresby 1820; Siggerud 1972; Imsland 1986), and yet another has been suggested to have occurred between AD 1650 and 1882 (Sylvester, 1975). Three Jan Mayen tephtras with ages of 2.3, 3.0 and 10.3 cal. ka BP are recorded in marine sediment cores (Gjerløw *et al.*, 2016). It is inferred that the summit crater of Beerenberg has also played a major role in the Holocene eruptive activity (Hawkins, 1963; Oftedahl, 1971; Roberts and Hawkins, 1971; Siggerud, 1972; Imsland, 1978, 1986), and

mapping of vents and lava flows led Imsland (1978) to suggest that a minimum of 75 eruptions have occurred across the entire island during the postglacial period.

In this study we present the first evidence of surface deformation, manifested as local uplift, associated with a volcanic eruption on Jan Mayen. Using stratigraphic exposures, GPR, radiocarbon dating and tephra geochemistry, we quantify the magnitude of the uplift and estimate its age. We also discuss whether a lake with a local stock of Arctic charr (*Salvelinus alpinus* L.) became landlocked by this uplift event. The result suggests that surface deformation may be an important variable of the Jan Mayen volcanic system, with potential for signalling the termination of periods of volcanic quiescence.

Setting

The island of Jan Mayen is located at the northern end of the Jan Mayen microcontinent some 700 km north of Iceland in the Norwegian–Greenland Sea (Fig. 1A). It is positioned just south of the Jan Mayen fracture zone that displaces the Mid-Atlantic ridge by some 200 km. The north part of the island is dominated by the majestic stratovolcano Beerenberg that reaches an elevation of 2277 m a.s.l. (Fig. 1B). This is the world's northernmost active volcano above sea level, and it is the surface expression of a large sub-sea volcanic province (Elkins *et al.*, 2016). Situated in the foothills of Beerenberg is the only proper lake on the island, Lake Nordlaguna (Fig. 1B).

*Correspondence: E. Larsen, as above.
E-mail: eiliv.larsen@ngu.no

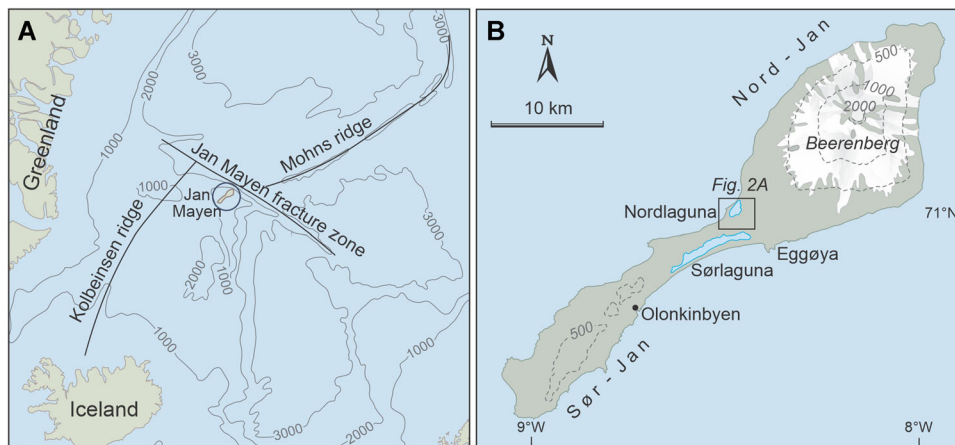


Figure 1. A. Jan Mayen (encircled) and its position relative to the mid-oceanic ridge system and the Jan Mayen fracture zone. Simplified after Eldholm and Sundvor (1980). B. Location of the Lake Nordlaguna area at the foothill of the Beerenberg volcano. [Color figure can be viewed at wileyonlinelibrary.com]

The lake is 1.6 km long with a lake surface 1–2 m a.s.l. It is predominantly bounded by steep mountain slopes (Figs. 2A and B). Three valleys enter the lake and to the west it is separated from the ocean by a beach barrier (Fig. 2A). The lake presently has no outlet to the ocean, and the inlets are only intermittent streams in the valleys.

Methods

Coastal cliffs and small, hand-dug stratigraphic sections were documented using sedimentological logs, sketches and photographs, and investigated for structural elements. Driftwood and whalebones were sampled for radiocarbon dating and, after returning from the field, stored in a cold room until analysis. Altitudes were measured by hand-levelling with a clinometer using the present sea level as a datum; an accuracy of ± 1 m is assumed. Geographic coordinates were determined using a hand-held GPS (Garmin gpsmap64st) with estimated horizontal accuracy of ± 5 m.

GPR uses electromagnetic fields to probe unconsolidated dielectric materials (Davis and Annan, 1989). We employed the Malå RTA system (Snake) which utilises a parallel end-fire antenna configuration (transmitting and receiving antennas in a row). The theoretical loss in data quality due to this antenna configuration is balanced by the opportunity to survey in rough terrain (Tassis *et al.*, 2015). The antenna frequency was 100 MHz, trace spacing was equal to 0.25 m and the time window equal to 220 ns, i.e. offering 11 m of depth coverage on a default 0.1 m/ns velocity. Processing was with EKKO_project v.4 software and included classic modules in GPR such as adjusting first break, dewowing, background subtraction DVL gaining and bandpass filtering. Positioning and topography were extracted from hand-levelled GPS tracks. Conversion to depth was achieved with a velocity equal to the default 0.1 m/ns value.

Radiocarbon dates (Table 1) were obtained by accelerator mass spectrometry at the Norwegian University for Science and Technology, Trondheim, Norway. Driftwood samples were determined to species level when not too degraded to be identified. Wood samples were cleaned with an alkali–acid–alkali treatment. Collagen was extracted from bone samples. The resulting material was prepared and measured according to Seiler *et al.* (2019). Radiocarbon ages are given as conventional ages relative to 1950 (Stuiver and Polach, 1977). Dates were calibrated using OxCal software (Bronk Ramsey *et al.*, 2013), with IntCal13 for terrestrial (wood) samples and Marine13 for marine (whale bone) samples (Reimer *et al.*, 2013). Whalebones were not

corrected for ΔR . The calibrated ages are reported in years AD with 1 and 2σ standard deviations.

Electron microprobe analyses on tephra were obtained on a Cameca SX100 electron microprobe at the Tephra Analysis Unit, University of Edinburgh, UK (six samples) and with the JXA-8530F JEOL Superprobe at Uppsala University, Sweden (four samples). Two of the samples were run at both laboratories. No significant differences in tephra glass geochemistry were observed between the instruments (Table 2). The Edinburgh samples were analysed using an accelerating voltage of 15 kV, a beam current of 2 nA for the major elements and 80 nA for the minor elements, and a beam diameter of 5 μm . Five primary calibration blocks were used for the calibration of the wavelength dispersive spectroscopy and two secondary glass standards, BCR2g and Lipari obsidian, were used to monitor drift in the analyses (Hayward, 2012). The Uppsala samples were analysed using an accelerating voltage of 15 kV, a beam current of 4 nA and a beam diameter of 10 μm . Glass standards reported in Jochum *et al.* (2006) were analysed for calibration and validation.

Sampling of Arctic charr was done on 15–16 August 2019 by using four overnight-set sinking benthic gillnets (10.0, 12.5, 15.5, 21.0 mm mesh). The care and use of the fish complied with the Government of Norway's animal welfare laws, guidelines and policies and was approved by the County Governor of Nordland (Permission nr. 2014/1086). The total length (L_T , mm), sex and maturity stage were determined in the field immediately after killing, and sagittal otoliths removed and stored in envelopes for later age determination following Grainger (1953).

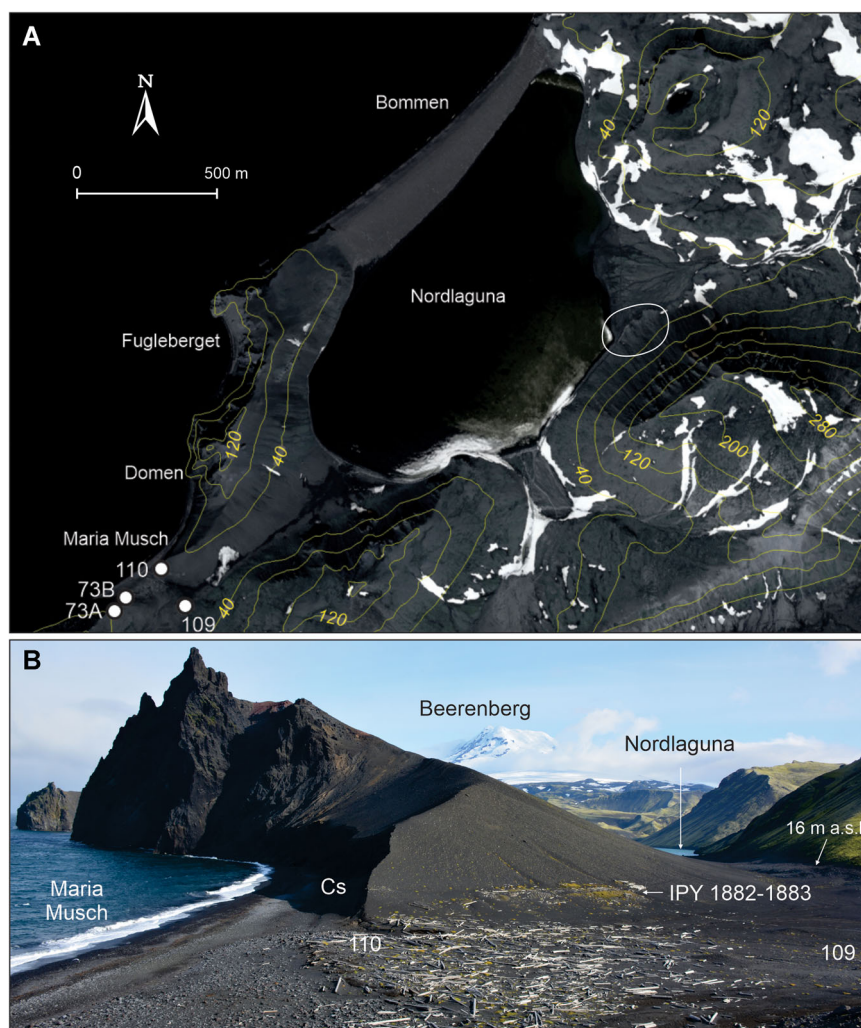
Lake outlets and Arctic charr

Though currently landlocked, Lake Nordlaguna (Figs. 2A and B) holds a stock of Arctic charr thought to have originated from migratory anadromous charr (Skreslett, 1973). Thus, it has been assumed that the Nordlaguna basin once had a passable connection to the sea. The two possible locations for such a connection are the beach barrier, Bommen (Fig. 2A), and the ca. 1 km long valley between Lake Nordlaguna and Maria Musch Bay.

The beach barrier

The beach barrier which separates Lake Nordlaguna from the ocean to the west (Fig. 2A) is about 1 km long, between 250 and 140 m wide and up to 5 m high. It is widest and highest in the southwest. The surface is composed of coarse sand to

Figure 2. A. Satellite image (3 September 2012, Kongsberg Satellite Services A.S.) of the Lake Nordlaguna area with location of sites (numbered). The area of Fig. 3B is encircled. B. Photo from the Maria Musch Bay (in the foreground) towards the northeast. The threshold between the Lake Nordlaguna and the bay at 16 m a.s.l. is marked with an arrow. The site of the International Polar Year 1882–1883 Austrian–Hungarian winter camp is also marked. [Color figure can be viewed at wileyonlinelibrary.com]



gravel, pebble and boulder-sized clasts; the largest up to 1 m in diameter. Boulders occur along the entire length of the barrier. Discrete beach ridges are found on the seaward side, and in places well-rounded pebbles are imbricated. On the lakeward side, shallow channels with levees of boulder-sized material occur perpendicular to the barrier (Fig. 3A). Large logs of driftwood are scattered across the surface of the barrier. The barrier is anchored at the foot of bedrock cliffs at either end. Bedrock is not exposed along the barrier.

The distribution of coarse grain sizes and wash-over channels indicates a swash-dominated system. This type of beach barrier is indicative of marine transgression (Forbes *et al.*, 1995). The local sea-level history in Jan Mayen is unknown. The entire island was, however, glaciated by an ice cap during the last glaciation (Lyså *et al.*, 2021). Given the island's limited area, the ice cap it supported was likely thin, suggesting that glacio-isostatic depression was moderate, leading to a marine transgression following deglaciation. On the valleyside east of Lake Nordlaguna, avalanche fans grade towards a base level some 2–3 m above the lake, i.e. 4–5 m a.s.l. (Figs. 2A and 3B). We suggest that sea level reached this level during the Tapes transgression about 8 to 6 ka ago (e.g. Bondevik *et al.*, 2019), and that the barrier formed during this interval of relative sea-level rise.

Deformed bedrock and overlying sediments

In Maria Musch Bay, where the valley enters the sea, a coastal cliff constitutes a prominent part of the northern shoreline (Figs. 2A and B). Southwards from this we dug three small sections (73A, 73B and 110) into the recent erosional escarpment, and one pit

(109) inside this escarpment (Figs. 2A and B). To extend the spatial extent of our observations of sediment distribution and tectonic elements, 19 GPR profiles were collected, two of which are included here (Figs. 6A, B and C).

The lowermost stratigraphic unit (Unit 1, Fig. 4A) is a bedded hyaloclastite exposed in the coastal cliff (Fig. 2B). At the cliff summit, 32 m a.s.l. it extends to the surface but is covered by unconsolidated sediment on either flank. Unit 1 is dissected by a complex pattern of faults and minor magma intrusions (Figs. 4B and C), none of which continues into the overlying unconsolidated sediment (Figs. 4B and C). Unit 2 is a cobble beach deposit extending from the lower right of the outcrop (Fig. 4D), and at least 250 m further to the southwest to site 73A (Fig. 2A). It is composed of well-rounded clasts up to boulder size, driftwood and whalebones. Unit 3 is a bedded sand and gravel dipping 15–30° towards the southwest (Figs. 4C and D). It lies on an erosional unconformity that crosscuts the bedrock, and it wedges out between the bedrock and the overlying unit in the upslope direction (Figs. 4C and D). In the lowest part of the section, sand of Unit 3 lies between and above the clasts, driftwood and whalebones of Unit 2 (Fig. 5A). The uppermost unit (4) is composed of finer grained sediment, compared with the underlying Unit 3, but on the slope it is mainly sand to gravel (Figs. 4C and D). The lower contact is an angular unconformity and the beds are gently dipping (<5°). Grain size decreases with decreasing elevation, i.e. downslope towards the bay. At sites 73A, B and 110 (Figs. 2A and B) the boundary between Units 3 and 4 is transitional (Fig. 5). At site 109 (Figs. 2A and B), Unit 4 is composed of four sequences of massive to laminated, medium

Table 1. Radiocarbon ages. Analyses were performed at the Norwegian University for Science and Technology, Trondheim, Norway. Dates were calibrated using OxCal software (Bronk Ramsey *et al.*, 2013), with IntCal13 for terrestrial samples and Marine13 for marine samples (Reimer *et al.*, 2013). Marine samples were not corrected for ΔR .

Lab Code	Sample no.	Site	Geographical position	Dated material	^{14}C Age BP	Calibrated age, a AD			
						68.2% probability		95.4% probability	
						From	To	From	To
Tra-10964	JM 2015-49	JM 73 A Maria Musch	70°59.642'N, 8°30.354'W	Driftwood	1785 ± 25	181	324	136	330
Tra-10963	JM 2015-48	JM 73 A Maria Musch	70°59.642'N, 8°30.354'W	Driftwood	1660 ± 20	355	415	341	421
Tra-10571	JM 2015-47	JM 73 A Maria Musch	70°59.642'N, 8°30.354'W	Driftwood, conifer	1425 ± 40	601	654	560	665
Tra-10966	JM 2015-52	JM 73 B Maria Musch	70°59.642'N, 8°30.354'W	Driftwood	1365 ± 25	649	666	633	684
Tra-10967	JM 2015-53	JM 73 B Maria Musch	70°59.642'N, 8°30.354'W	Driftwood	1430 ± 20	612	646	587	655
Tra-10968	JM 2015-55	JM 73 B Maria Musch	70°59.642'N, 8°30.354'W	Driftwood	1450 ± 10	604	633	586	645
Tra-10573	JM 2015-54	JM 73 B Maria Musch	70°59.642'N, 8°30.354'W	Driftwood, indefinite	1355 ± 20	654	668	647	680
Tra-10965	JM 2015-50	JM 73 A Maria Musch	70°59.642'N, 8°30.354'W	Driftwood	1130 ± 30	887	970	777	987
Tra-10572	JM 2015-51	JM 73 B Maria Musch	70°59.642'N, 8°30.354'W	Whale bone	1560 ± 30	785	858	762	900
Tra-10969	JM 2015-56	JM 73 B Maria Musch	70°59.642'N, 8°30.354'W	Driftwood	1120 ± 25	894	969	882	989
Tra-11134	JM 2016-13	JM 110 Maria Musch	70°59.689'N, 8°30.166'W	Driftwood, <i>Pinus</i> sp.	840 ± 20	1169	1223	1163	1253
Tra-11135	JM 2016-14	JM 110 Maria Musch	70°59.689'N, 8°30.166'W	Driftwood, <i>Picea/Larix</i> sp.	885 ± 20	1057	1205	1046	1218
Tra-11136	JM 2016-15	JM 110 Maria Musch	70°59.689'N, 8°30.166'W	Driftwood, <i>Pinus</i> sp.	875 ± 15	1158	1206	1052	1218
Tra-13153	JM 2017-51	JM 110 Maria Musch	70°59.689'N, 8°30.166'W	Driftwood, <i>Salix/Populus</i> sp.	310 ± 15	1523	1642	1515	1645
Tra-13155	JM 2017-54	JM 110 Maria Musch	70°59.689'N, 8°30.166'W	Whale bone	770 ± 15	1492	1553	1478	1617
Tra-13154	JM 2017-52	JM 110 Maria Musch	70°59.689'N, 8°30.166'W	Driftwood, <i>Picea/Larix</i> sp.	280 ± 15	1529	1650	1522	1660

Table 2. Tephra geochemistry from electron microprobe analyses. Analyses were performed in Uppsala, Sweden (Upp) and Edinburgh, UK (Ed). Some samples were run at both laboratories. All samples are interpreted as Eggøya tephra (E) when comparing with the 1732 Eggøya tephra from Gjerløw *et al.* (2015).

Sample no.	Site	Geographical position	analyses (glass)	Mean \pm 1 SD	Na ₂ O	SiO ₂	Al ₂ O ₃	MgO	K ₂ O	CaO	TiO ₂	P ₂ O ₅	FeO	MnO	Total	Na + K	Comments
JM2016-17	JM 110	70°59.689'N, 8°30.166'W	5	mean SD	3.39 0.08	46.51 0.70	15.65 0.35	4.32 0.19	3.01 0.28	8.93 0.54	3.24 0.10	0.70 0.06	10.09 0.32	0.24 0.06	96.07 1.25	6.39	E Upp
JM2016-18	JM 110	70°59.689'N, 8°30.166'W	10	mean SD	3.54 0.34	47.09 1.13	15.62 0.50	4.39 0.27	2.84 0.30	8.85 0.58	3.20 0.14	0.75 0.10	9.82 0.56	0.22 0.09	96.32 2.16	6.38	E Upp
JM2016-4	JM 109	70°59.640'N, 8°29.956'W	7	mean SD	3.52 0.27	46.74 0.64	15.97 0.13	4.58 0.18	2.81 0.14	9.29 0.39	3.12 0.15	0.67 0.04	9.92 0.47	0.18 0.06	96.80 1.27	6.33	E Upp
JM2016-4	JM 109	70°59.640'N, 8°29.956'W	9	mean SD	3.59 0.33	47.82 1.03	16.13 0.51	4.44 0.19	3.04 0.15	9.35 0.28	3.21 0.15	0.59 0.02	10.32 0.42	0.21 0.02	98.69 1.49	6.63 0.28	E Ed
JM2016-6A	JM 109	70°59.640'N, 8°29.956'W	29	mean SD	3.58 0.24	48.48 0.74	16.13 0.63	4.16 0.34	3.16 0.23	9.27 0.44	3.25 0.21	0.64 0.07	10.22 0.48	0.21 0.02	99.11 0.71		E Ed
JM2016-6B	JM 109	70°59.640'N, 8°29.956'W	34	mean SD	3.47 0.14	48.12 0.62	16.01 0.29	4.20 0.22	3.13 0.22	9.27 0.30	3.27 0.08	0.63 0.05	10.22 0.30	0.21 0.01	98.55 0.67		E Ed
JM2016-9	JM 109	70°59.640'N, 8°29.956'W	42	mean SD	3.55 0.24	47.85 0.88	15.88 0.44	4.31 0.27	3.12 0.28	9.19 0.45	3.26 0.12	0.67 0.04	10.22 0.41	0.21 0.01	98.26 1.13		E Ed
JM2016-10	JM 109	70°59.640'N, 8°29.956'W	40	mean SD	3.51 0.18	48.02 0.79	15.90 0.31	4.16 0.24	3.12 0.24	9.25 0.49	3.25 0.08	0.63 0.03	10.21 0.34	0.21 0.01	98.28 0.85		E Ed
JM2016-11	JM 109	70°59.640'N, 8°29.956'W	6	mean SD	3.56 0.17	46.58 0.32	15.68 0.19	4.19 0.29	2.99 0.24	8.97 0.46	3.21 0.16	0.77 0.08	9.85 0.44	0.21 0.03	95.99 0.40	6.55	E Upp
JM2016-11	JM 109	70°59.640'N, 8°29.956'W	7	mean SD	3.76 0.14	47.30 0.82	16.14 0.56	4.37 0.11	2.94 0.10	9.45 0.33	3.15 0.09	0.57 0.02	10.15 0.21	0.20 0.01	98.04 1.40	6.70 0.18	E Ed
			81	mean SD	3.53 0.11	47.53 0.53	16.22 0.21	4.27 0.15	3.06 0.13	9.32 0.28	3.24 0.05	0.67 0.02	10.35 0.30	0.22 0.01	98.41	6.59	Gjerløw <i>et al.</i> (2015)

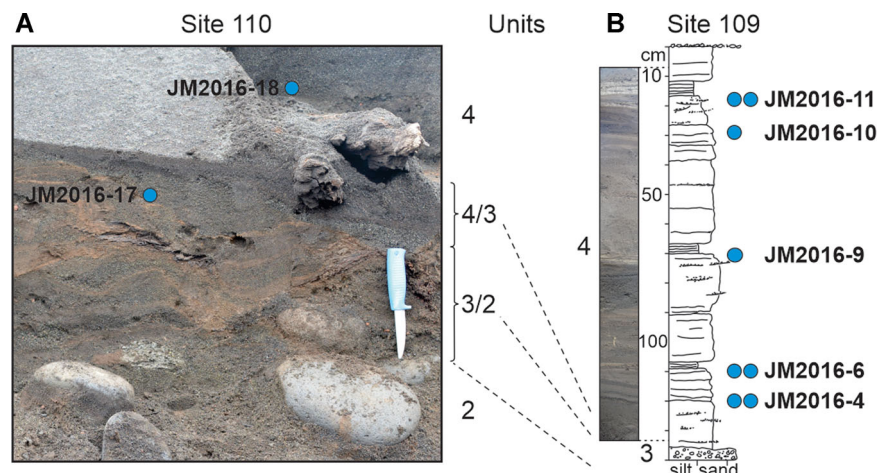


Figure 3. A. Wash-over channels on the lake side of the beach barrier, Bommen (see Fig. 2A). Distance between levee crests is about 3 m. B. Lower parts of avalanche fans next to the eastern shore of Lake Nordlaguna (see Fig. 2A). [Color figure can be viewed at wileyonlinelibrary.com]



Figure 4. A. Overview of north-south section in the northern part of the Maria Musch Bay, see Figs. 2B and 5A for location. Panels B–D are framed. B. Numerous faults (dotted) in the rock (Unit 1) below undisturbed Eggøya tephra (unit 4). C. Contact (stippled) between faulted hyaloclastite (Unit 1) and sandy-gravelly sediments (Unit 3) eroded from the developing slope. The contact to finer, post-faulting sediments above (Unit 4) is shown by arrows. D. The architecture in the southern part of the hill. The faulted rock (Unit 1) is overlain by a wedge of the sandy Unit 3, which again is covered by a blanket of the fine-grained sediments of Unit 4. The unit boundaries are stippled. Unit 2, gravel containing boulders, driftwood and whalebones is located stratigraphically between Units 1 and 3 and found in the lower right of the picture. Fig. 5A is framed. [Color figure can be viewed at wileyonlinelibrary.com]

Figure 5. Sites 109 and 110 located about 200 m apart (see Fig. 2B) with stratigraphic position of tephra samples. Unit numbers are indicated. A. Site 110 with well-rounded cobbles and boulders along with driftwood and whalebones (Unit 2) covered by sand (Units 3 and 4). B. Log and photo representing the pit, site 109. [Color figure can be viewed at wileyonlinelibrary.com]



to fine sand. The three lowermost sequences are topped with finely laminated silt to fine sand (Fig. 5B). The uppermost few centimetres of the site 109 pit is composed of medium sand with a coarse sand to gravel lag. Across the topographic high to the north (Fig. 4A), Unit 4 rests directly on bedrock (Unit 1) and is composed of laminated silt to fine sand (Fig. 4B).

GPR profile 273 extends from the coast of the marine bay to the valley, starting close to the coastal section (Fig. 6A). Profile 270 starts at the endpoint of profile 273 and runs along the valley floor across its highest point. Maximum penetration was approximately 10 m. Poorly defined reflectors, as seen in profile 273 from about 7 m depth, are probably caused by brackish groundwater limiting penetration (Fig. 6B) (Jol *et al.*, 1996; Tillmann and Wunderlich, 2012). Both profiles may be divided into three units. The lowermost and thickest unit exhibits well-defined reflectors having a channelised and subparallel pattern. Several sub-vertical faults with offset up to about 0.5 m are identified, none extending into Units 3 and 4 (Figs. 6B and C). Thus, this deepest unit can easily be correlated with Unit 1 in the adjacent coastal section (Fig. 4).

In profile 273, the unit above exhibits an irregular pattern of reflectors, whereas a continuous and subparallel pattern of reflectors with low-angle wedges forming subunits is seen in profile 270 (Figs. 6B and C). The unit thickens downslope on either side of the high point in the valley. Across the high point in the valley, the unit is very thin or completely absent (Fig. 6C). This unit is correlated with Unit 3 of the coastal section based on its geometry, structures and stratigraphic position. The uppermost unit, corresponding to Unit 4 in the sections, is composed of weakly developed internal reflectors and is separated from the underlying unit by a well-defined reflector (Figs. 6B and C). This is consistent with this unit being composed of somewhat finer grained material than the unit below.

Both the coastal section and GPR profile 270 cross topographic highs that are defined by the bedrock of Unit 1 (Figs. 4 and 6C). In the GPR, the reflectors show a step-like pattern interpreted as two opposing sets of normal faults with apparent offset of about 0.5 m for individual faults. The orientation of the inferred faults defines a former centre of

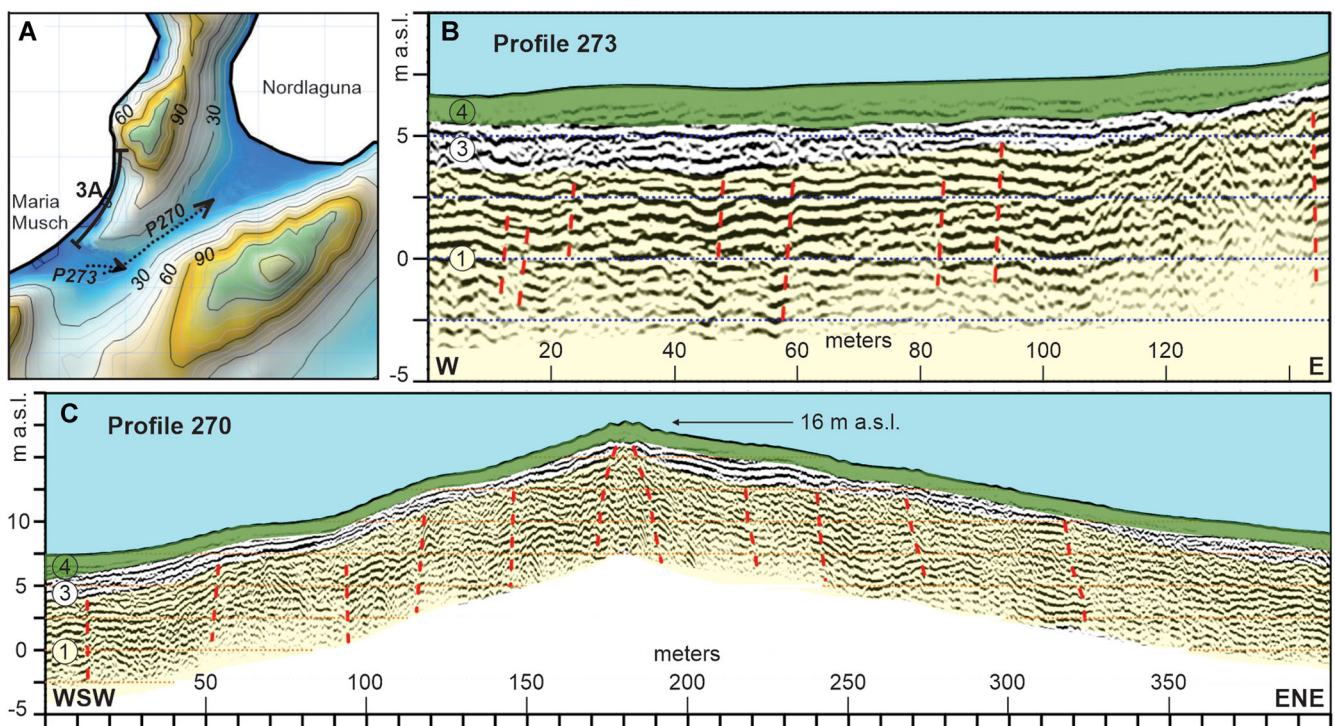


Figure 6. A. Location of the GPR profiles in Panels B and C and the coastal section in Fig. 4A. B and C. GPR profiles showing steeply inclined faults, some of which are indicated by red stippling. [Color figure can be viewed at wileyonlinelibrary.com]

uplift rising to about 14 m a.s.l. at the valley threshold (Fig. 6C). In the coastal section, the faulted bedrock attains a maximum elevation of 32 m a.s.l. and exhibits a similar uplifted structure. This suggests a horst- or dome-like structure extending between the high points. In any case, this is the major topographic control between the lake and the bay. The absence of Unit 3 across the topographic highs, the downslope thickening, and the reflection pattern in the GPR data (Figs. 4C, D and 6C), shows that deposition of the unit was by downslope mass wasting initiated by tectonic uplift. The source may have been material reactivated on the steepening slope during uplift and/or material breaking loose from the rising bedrock. These deposits cover beach gravel, driftwood, and whale bones (Unit 2) on the adjacent beach. Thus, the driftwood and whalebones predate these sediments and thus the uplift event. When Unit 4 started to form, uplift had slowed down or ceased. This may be seen in the northern part of the coastal section where undisturbed, laminated sediments of the unit drape the faulted bedrock (Fig. 4B) but it is also evident from the pit and the GPR profiles (Figs. 5 and 6). This sediment was also deposited by downslope mass wasting. The finer grain size compared with the underlying Unit 3 is attributed to a deceleration in uplift activity as the tectonism waned and eventually ceased.

Age of tectonic deformation

Sixteen radiocarbon dates (2 whalebones, 14 driftwood) were obtained from sites 73A, 73B and 110 (Fig. 2A; Table 1), all from Unit 2 (Fig. 5A). The dates span approximately AD 130 to 1660 (Fig. 7). For driftwood samples, the calibrated radiocarbon age represents a maximum age for the death of the tree, because samples were degraded, and many tree rings might have been missing. The driftwood on Jan Mayen originates either in northwest Russia or in Siberia (Johansen, 1998). Westward transport to Fram Strait by the Transpolar Drift Stream takes only a few years (Pfirman *et al.*, 1997). This may, thus, be considered negligible with regards to evaluating the

time of beach stranding. The youngest sample yielded an age of AD 1522–1660 within 95.4% probability (Fig. 6 and Table 1) and is the closest maximum-limiting age for the land-deforming event. The uplift is clearly older than AD 1882, as the winter quarters for the 1882–1883 Austrian–Hungarian International Polar Year Expedition (Berwerth, 1886) were built on the uplifted slope where the ruins can still be found (Fig. 2B). Tephra analysed from the pit (site 109) and from site 110 are all similar in major-element composition (Figs. 5 and 7; Table 2) and identical to tephra from the AD 1732 Eggøya eruption, e.g. MgO between 4.2 and 4.6 wt% and TiO₂ between 3.1 and 3.3 wt% (Fig. 7; Gjerløw *et al.*, 2015). These values distinguish the Eggøya tephra from all other published Holocene tephras from Jan Mayen (Gjerløw *et al.*, 2015, 2016), and we conclude that our samples are correlative with Eggøya. Tephra sample 17 (Fig. 5A) was collected from the transition zone between Units 3 and 4. This contact is poorly defined and may be due to some redeposition. It was previously concluded that deposition of Unit 3 took place during tectonic uplift. The upper transition of the unit containing Eggøya tephra may indicate that uplift persisted until after the AD 1732 eruption had started (Fig. 5A). On top of the coastal section, undisturbed tephra of Unit 4 is situated directly on faulted bedrock (Fig. 4B), and in the pit tephra is found undisturbed within Unit 4 (Figs. 5B and 7). Thus, the available data allow for a scenario in which uplift began just prior to the Eggøya AD 1732 eruption, continued during the eruption, and ended before the eruption ceased (Fig. 7).

The population of landlocked Arctic charr

Body length, age, sex and stage of maturation of Arctic charr in Lake Nordlaguna were investigated to test whether the population had reached a typical climax structure after it was landlocked in 1732. We caught 116 fish ranging in size from 104 to 700 mm (mean 159 mm), with the majority (93%) being less than 200 mm. Ages ranged from 2 to 19 years (mean 4.8 years) and were numerically dominated by the younger (#7) age classes. Of 97 individuals where sex could be determined, 46% were males and 54% females. Most fish were sexually mature (males, 80%, females 85%). Treating the 19 non-sexed individuals with poorly developed gonads as immature fish, the overall proportion of mature fish was 69%, with ages ranging from 3 to 19 years (mean 5.1 years).

Discussion

Skreslett (1973) suggested that the beach barrier (Fig. 2A) was formed due to land uplift, i.e. during regression, some 1500–4000 years ago, and that this closed the connection with the sea that caused the Arctic charr to become landlocked. As such barriers normally form during transgressions (Forbes *et al.*, 1995), we previously suggested that the barrier formed during the Holocene Tapes transgression, but this does not imply that this was the cause of landlocking. Conversely, the data presented here suggest that a passage to the sea was open after the barrier had formed, and that it was blocked due to uplift in the Maria Musch Bay – Lake Nordlaguna valley area, resulting from the Eggøya AD 1732 eruption. Over a stretch of some 250 m, between sites 73A and 110 (Fig. 2A), the beach deposit, Unit 2, is situated at 1.5–2 m a.s.l. (Fig. 5). This shows both that the pre-uplift beach elevation was at about the elevation of the present beach level, and that it was not uplifted by the 1732 event. Assuming a pre-uplift low gradient river or tidal channel connecting the lake with the sea, the elevation of the bedrock surface at the highest point in the valley (14 m a.s.l.) can be

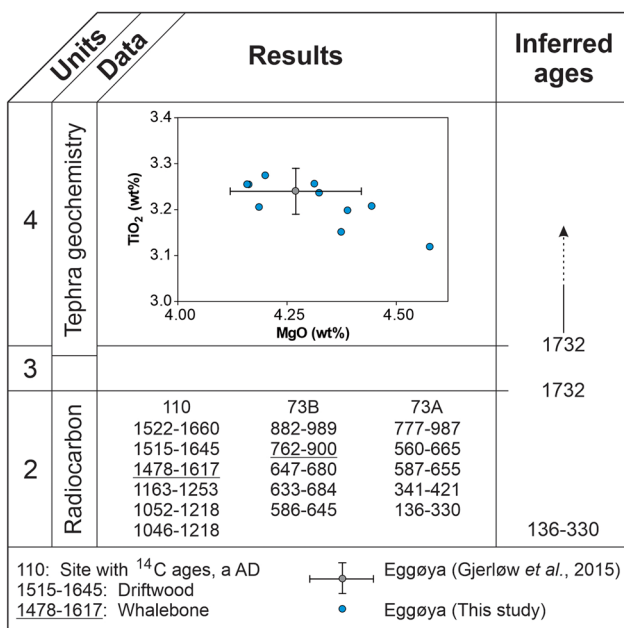


Figure 7. Chronology of Units 2–4. Ages based on radiocarbon dates are given in (calibrated) calendar a AD within 95.4% probability. The full radiocarbon data are given in Table 1. A biplot of mean values of MgO vs. TiO₂ in samples from sites 109 and 110 (Fig. 5) are compared with analyses of the Eggøya AD 1732 tephra (mean and 1σ of 81 analyses; Gjerløw *et al.*, 2015). The full geochemical data can be found in Table 2.

considered an approximation of the magnitude of vertical uplift that took place. From this, it is inferred that this uplift blocked the lake–sea connection, rendering the lake landlocked and thereby denying its stock of Arctic charr access to the ocean. Uplift of comparable magnitude was recorded within the Campi Flegrei caldera in Italy before an eruption in 1538 (Dvorak and Mastrolorenzo, 1991; D’Argenio *et al.*, 2004). The resulting geometry of the deformation in Jan Mayen is somewhat unclear from available data, but it may resemble a dome- or horst-like structure (Fig. 6C). The fault pattern and associated magma intrusions (Fig. 4B) suggest that intrusion of a shallow magma body displaced the overlying rock causing the documented land surface deformation.

An eruption in Jan Mayen in 1732 was observed at distance by German whalers (Anderson, 1746), but it was not until the work of Gjerløw *et al.* (2015) that this observation could be assigned definitively to the eruption forming Eggøya on the east coast of the island (Fig. 1B). The distance between Eggøya and Maria Musch Bay is about 4.5 km. However, we suggest there is a causal linkage because tephra from the eruption can be tied into the sediment succession documenting the uplift in Maria Musch Bay. The Eggøya eruption took place at shallow (~20 m) water depth. We infer that an ash cloud formed in the atmosphere above the vent when the eruption broke through sea level. The lowermost tephra from Eggøya is found in the transition between Units 3 and 4 (Fig. 7), suggesting that uplift was ongoing as the eruption began. However, most observations are of tephra in undisturbed positions overlying Units 2 and 3, indicating that the eruption continued after the uplift ceased. This timing and the intrusion of magma into the tectonised bedrock, strongly indicates that during the volcanic unrest causing the formation of Eggøya some magma was routed upwards to the Lake Nordlaguna area (Fig. 8). This is much like the satellites to the 1963 Surtsey eruption off the coast of Iceland (Kokelaar, 1983), but without a vent opening in the case of Jan Mayen. The linkage of this tectonic event to the Eggøya eruption suggests that this was a short-lived,

episodic event. The duration of the deformation cannot be determined, but some weeks to months may be envisaged as maximum if compared with other areas (Sigurdsson, 1980; Dvorak and Mastrolorenzo, 1991; Albert *et al.*, 2016; Lamolda *et al.*, 2017; Martí *et al.*, 2013a, b). The results presented here are the first to document land deformation associated with volcanic activity in the Jan Mayen volcanic province. This also emphasises that surface deformation may be an important part in case of reactivation of the Jan Mayen volcanic system, with the potential for signalling the termination of the current volcanic quiescence. The two most recent volcanic eruptions in 1970 and 1985 were effusive with lava flows extending the northernmost coastline of the island (Siggerud, 1972; Imsland, 1986). Land deformation associated with these eruptions has not been studied.

The test fishery of Lake Nordlaguna confirmed the finding by Skreslett (1973) of an established population of Arctic charr that was both growing and reproducing. The size- and age-structure mirrors that of the typical unexploited populations as characterised by Johnson (1976) and Power (1978), which are noted for their high degree of clustering around length- and age-frequency modal values; the so-called ‘climax condition’ (Johnson, 1976). The clustering and small proportion of older, larger individuals has been interpreted as characteristic of populations limited by resource availability (Johnson, 1976; Power 1978). Although not specified, the achievement of the ‘climax condition’ is thought to be a product of the consistent operation of ecological forces over extended periods of time (Johnson, 1976) and driven by the prevalence of cannibalism. Work with translocated populations of Arctic charr, however, suggest that significant structural changes within populations occurring in response to ecological opportunities or constraints can occur quickly (Michaud *et al.*, 2008). This is consistent with the rapid change from a largely anadromous population to the climax lacustrine population found in Lake Nordlaguna and as would be implied by the dates for the closing of anadromous access as suggested here.

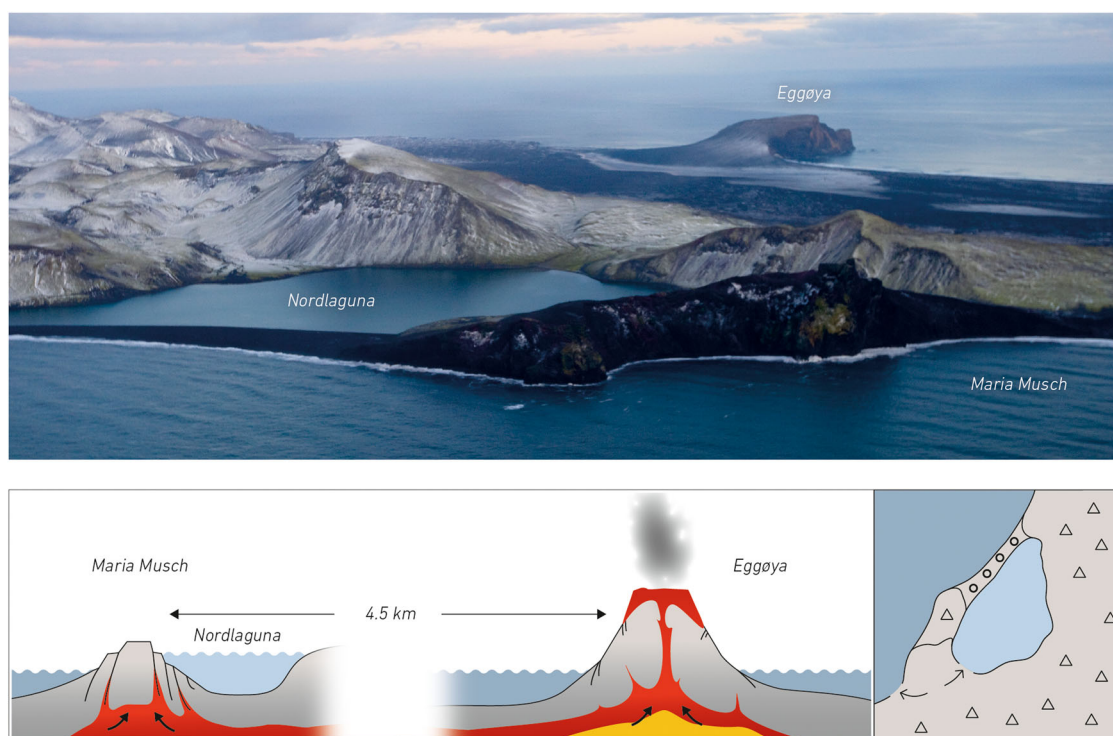


Figure 8. Above is an overview photo looking southeast from the Lake Nordlaguna area towards the Eggøya tuff cone. Photo reproduced with permission from NTB. Lower left is a cartoon illustrating the eruption causing the formation of Eggøya and the associated uplift in the lake Nordlaguna caused by upwards flowing of magma. This led to landlocking of proto-Nordlaguna to form the present lake (lower right). [Color figure can be viewed at wileyonlinelibrary.com]

Conclusions

- A land surface deformation expressed as vertical uplift of about 14 m has been documented for an area on the west coast of the island of Jan Mayen.
- Radiocarbon- and tephrochronology tie the uplift to a historically known Surtseyan eruption in 1732 forming the island Eggøya off Jan Mayen's east coast. It is likely that the uplift started just prior to the eruption and ended before the eruption had ceased.
- The established chronology and coupling to the Eggøya eruption show that the uplift was episodic rather than part of a long-term tectonic trend.
- This is the first record of land surface deformation in Jan Mayen that can be linked to a known eruption event. We attribute the uplift to intrusion of shallow magma associated with this eruption.
- The uplift caused a coastal, freshwater lake to lose its outlet to the sea and become landlocked, within which a typical climax population structure of Arctic charr has developed.

Acknowledgements. Funding was provided by the Research Council of Norway (Grant no. 244135/E10) to A.L. and by the Geological Survey of Norway. The County Governor of Nordland, CYFOR CTO NORD and the staff at the Jan Mayen station gave permission and logistical support. Irene Lundqvist and Mads C. Rasmussen made line drawings. Helene Svarva analysed driftwood samples. Aslak Darre Sjursen participated in the test-fishing, and Lars Rønning aged the Arctic charr. Svante Björck, Jan Mangerud and Thomas Lakeman read the manuscript critically. T.L. also corrected the English language. We thank Karoly Nemeth and an anonymous reviewer for their constructive suggestions to the manuscript.

Data Availability Statement

The data that support the findings of this study are all included in this article.

References

Albert H, Costa F, Martí J. 2016. Years to weeks of seismic unrest and magmatic intrusions precede monogenetic eruptions. *Geology* **44**: 211–214.

Anderson J 1746. Nachrichten von Island, Grönland und der Strasse Davis. Hamburg.

Berwerth F 1886. Über Gesteine von Jan Mayen. Die Österreichische Polarstation Jan Mayen 3, Band 8, Teil 1–20.

Bondevik S, Lødøen TK, Tøssebro C *et al.* 2019. Between winter storm surges - Human occupation on a growing Mid-Holocene transgression maximum (Tapes) beach ridge at Longva, Western Norway. *Quaternary Science Reviews* **215**: 116–131.

Bronk Ramsey C, Scott EM, van der Plicht J. 2013. Calibration for archaeological and environmental terrestrial samples in the time range 26–50 ka cal BP. *Radiocarbon* **55**: 2021–2027.

D'Argenio A, Pescatore T, Senatore MR. 2004. Sea-level change and volcano-tectonic interplay. The Gulf of Pozzuoli (Campi Flegrei, Eastern Tyrrhenian Sea) during the last 39 ka. *Journal of Volcanology and Geothermal Research* **133**: 105–121.

Davis JL, Annan AP 1989. Borehole radar sounding in CR-6, CR-7 and CR-8 at Chalk River, Ontario: Technical Record TR-401, Atomic Energy of Canada Ltd.

Dvorak JJ, Mastrolorenzo G 1991. The mechanism of recent crustal movements in Campi Flegrei caldera, Southern Italy. *Geological Society of America Special Paper* **263**: 1–47.

Eldholm O, Sundvor E. 1980. The continental margins of the Norwegian-Greenland Sea: recent results and outstanding problems. *Philosophical Transactions of the Royal Society of London A* **294**: 77–86.

Elkins LJ, Hamelin C, Blichert-Toft J *et al.* 2016. North Atlantic hotspot-ridge interaction near Jan Mayen Island. *Geochemical Perspectives Letters* **2**: 55–67.

Forbes DL, Orford JD, Carter RWG *et al.* 1995. Morphodynamic evolution, self-organisation, and instability of coarse-clastic barriers on paraglacial coasts. *Marine Geology* **126**: 63–85.

Gjerløw E, Hafliðason H, Pedersen RB. 2016. Holocene explosive volcanism of the Jan Mayen (island) volcanic province, North-Atlantic. *Journal of Volcanology and Geothermal Research* **321**: 31–43.

Gjerløw E, Höskuldsson A, Pedersen RB. 2015. The 1732 Surtseyan eruption of Eggøya, Jan Mayen, North-Atlantic: deposits, distribution, chemistry and chronology. *Bulletin of Volcanology* **77**: 14.

Grainger EH. 1953. On the Age, Growth, Migration, Reproductive Potential and Feeding Habits of the Arctic Char (*Salvelinus alpinus*) of Frobisher Bay, Baffin Island. *Journal of the Fisheries Research Board of Canada* **10**: 326–370.

Gudmundsson MT, Pálsson F, Björnsson H *et al.* 2002. The hyaloclastite ridge formed in the 1996 eruption in Gjalp, Vatnajökull, Iceland: present day shape and future preservation. In *Volcano-Ice interaction on Earth and Mars*, Smellie JL, Chapman MG. (eds). *Geological Society, London, Special Publications* **202**: 319–335.

Hawkins TRW. 1963. Agglutinate in north Jan Mayen. *Geological Magazine* **100**(2): 156–163.

Hayward C. 2012. High spatial resolution electron probe micro-analysis of tephra and melt inclusions without beam-induced chemical modification. *The Holocene* **22**: 119–125.

Imsland P 1978. The Geology of the Volcanic Island Jan Mayen, Arctic Ocean. *Nordic Volcanological Institute* **78**, No. 13, University of Iceland, Reykjavik, 74 pp.

Imsland P. 1986. The volcanic eruption on Jan Mayen, January 1985: Interaction between a volcanic island and a fracture zone. *Journal of Volcanology and Geothermal Research* **28**: 45–53.

Jochum KP, Stoll B, Herwig K *et al.* 2006. MPI-DING reference glasses for in situ microanalysis: New reference values for element concentrations and isotope ratios. *Geochemistry Geophysics Geosystems* **7**(2): Q02008.

Johansen S. 1998. The origin and age of driftwood on Jan Mayen. *Polar Research* **17**: 125–146.

Johnson L. 1976. Ecology of arctic population of lake trout, *Salvelinus namaycush*, lake white fish, *Coregonus clupeaformis*, Arctic charr, *S. alpinus*, and associated species in unexploited lakes of the Canadian Northwest Territories. *Journal of the Fisheries Research Board of Canada* **33**: 2459–2488.

Jol HM, Smith DG, Meyers RA. 1996. Digital Ground Penetration Radar: A new geophysical tool for coastal barrier research (examples from the Atlantic, Gulf and Pacific coasts, U.S.A.). *Journal of Coastal Research* **12**: 960–968.

Kokelaar BP. 1983. The mechanism of Surtseyan volcanism. *Journal of the Geological Society* **140**: 939–944.

Lamolda H, Felpeto A, Bethencourt A. 2017. Time lag between deformation and seismicity along monogenetic volcanic unrest periods: The case of El Hierro Island (Canary Islands). *Geophysical Research Letters* **44**: 6771–6777.

Lyså A, Larsen E, Anjar J *et al.* 2021. The last glaciation of the Arctic volcanic island Jan Mayen. *Boreas* **50**: 6–28.

Manville V, Nemeth K, Kano K. 2009. Source to sink: A review of three decades of progress in the understanding of volcanoclastic processes, deposits, and hazards. *Sedimentary Geology* **220**: 136–161.

Martí J, Castro A, Rodriguez C *et al.* 2013a. Correlation of Magma Evolution and Geophysical Monitoring during the 2011–2012 El Hierro (Canary Islands) Submarine Eruption. *Journal of Petrology* **54**: 1349–1373.

Martí J, Pinel V, Lopez C *et al.* 2013b. Causes and mechanisms of the 2011–2012 El Hierro (Canary Islands) submarine eruption. *Journal of Geophysical Research-Solid Earth* **118**: 823–839.

Martí J, GropPELLI G, Brum, da Silveira A. 2018. Volcanic stratigraphy: A review. *Journal of Volcanology and Geothermal Research* **357**: 68–91.

Michaud W, Power M, Kinnison M. 2008. Tropically mediated divergence of Arctic charr (*Salvelinus alpinus* L.) populations in contemporary time. *Evolutionary Ecology Research* **10**: 1051–1066.

Nemeth K, Palmer J. 2019. Geological mapping of volcanic terrains: Discussion on concepts, facies models, scales, and resolutions from

- New Zealand perspective. *Journal of Volcanology and Geothermal Research* **385**: 27–45.
- Oftedal CG. 1971. Vulkanutbruddet på Jan Mayen høsten 1970. *Det Norske Videnskapsakademi i Oslo Årbok* **1971**: 36–37.
- Pfirman SL, Colony R, Nürnberg D *et al.* 1997. Reconstructing the origin and trajectory of drifting Arctic sea ice. *Journal of Geophysical Research: Oceans* **102**: 1275–1286.
- Pistolesi M, Bertagnini A, Di Roberto A *et al.* 2020. Tsunami and tephra deposits record interactions between past eruptive activity and landslides at Stromboli, volcano, Italy. *Geology* **48**: 436–440.
- Power G. 1978. Fish population structure in arctic lakes. *Journal of the Fisheries Research Board of Canada* **35**: 53–59.
- Reimer P, Bard E, Bayliss A *et al.* 2013. IntCal13 and Marine13 radiocarbon age calibration curves 0–50,000 years cal BP. *Radiocarbon* **55**: 1869–1887.
- Roberts B, Hawkins TRW. 1971. The petrology of the volcanic and intrusive rocks of Nord-Jan, Jan Mayen. *Norsk Polarinstitutt Årbok 1970*.
- Scoresby W Jr. 1820. An account of the Arctic regions, with a history and description of the Northern whale-fishery. A Constable & Co, Edinburgh.
- Seiler M, Grootes P, Haasaker J *et al.* 2019. Status report of the Trondheim. *Radiocarbon Laboratory. Radiocarbon* **61**: 1963–1972.
- Siggerud T. 1972. The volcanic eruption on Jan Mayen 1970. *Norsk Polarinstitutt Årbok for 1970*: 5–18.
- Sigurdsson O. 1980. Surface deformation of the Krafla Fissure Swarm in two Rifting events. *Journal of geophysics* **47**: 154–159.
- Skreslett S. 1973. The Ecosystem of the Arctic Lake Nordlaguna, Jan Mayen Island. III. Ecology of Arctic Char, *Salvelinus alpinus* (L.). *Astarte* **6**: 43–54.
- Smellie JL, Rocchi S, Johnson JS *et al.* 2018. A tuff cone erupted under frozen-bed ice (Northern Victoria Land, Antarctica): linking glacio-volcanic and cosmogenic nuclide data for ice sheet reconstructions. *Bulletin of Volcanology* **80**: 12.
- Stuiver M, Polach H. 1977. Discussion. Reporting of ¹⁴C Data. *Radiocarbon* **19**(3): 355–363.
- Sylvester AG. 1975. History and surveillance of volcanic activity on Jan Mayen island. *Bulletin of Volcanology* **39**(2): 1–23.
- Tassis G, Rønning JS, Hansen L *et al.* 2015. Comparison between Sensors & Software and Malå GPR equipment based on test measurements at Bøaøyna, Stryn Municipality, Norway. NGU Report 2015.014 (41 pp.).
- Tillmann T, Wunderlich J. 2012. Ground penetrating radar in coastal environments: Examples from the islands of Sylt and Amrum. *Bremer Beiträge zur Geographie und Raumplanung* **44**: 60–77.
- Zernack AV, Cronin SJ, Neall VE *et al.* 2011. A medial to distal volcaniclastic record of an andesite stratovolcano: detailed stratigraphy of the ring-plain succession of south-west Taranaki, New Zealand. *International Journal of Earth Sciences* **100**: 1937–1966.